Observation of Open-Orbit Fermi Surface Topology in Extremely Large Magnetoresistance Semimetal $MoAs_2$

R. Lou,[1] Y. F. Xu,[2,3] L.-X. Zhao,[2,3] Z.-Q. Han,[1,2] P.-J. Guo,[1] M. Li,[1,4] J.-C. Wang,[1] B.-B. Fu,[2,3] Z.-H. Liu,[5] Y.-B. Huang,[4] P. Richard,[2,3,6] T. Qian,[2,6] K. Liu,[1] G.-F. Chen,[2,3,6] H. M. Weng,[2,6] H. Ding,[2,3,6] and S.-C. Wang[1,*]

[1]*Department of Physics and Beijing Key Laboratory of Opto-electronic Functional Materials & Micro-nano Devices, Renmin University of China, Beijing 100872, China*
[2]*Beijing National Laboratory for Condensed Matter Physics, and Institute of Physics, Chinese Academy of Sciences, Beijing 100190, China*
[3]*School of Physical Sciences, University of Chinese Academy of Sciences, Beijing 100190, China*
[4]*Shanghai Synchrotron Radiation Facility, Shanghai Institute of Applied Physics, Chinese Academy of Sciences, Shanghai 201204, China*
[5]*State Key Laboratory of Functional Materials for Informatic, SIMIT, Chinese Academy of Sciences, Shanghai 200050, China*
[6]*Collaborative Innovation Center of Quantum Matter, Beijing, China*

While recent advances in band theory and sample growth have expanded the series of extremely large magnetoresistance (XMR) semimetals in transition metal dipnictides $TmPn_2$ (Tm = Ta, Nb; Pn = P, As, Sb), the experimental study on their electronic structure and the origin of XMR is still absent. Here, using angle-resolved photoemission spectroscopy combined with magnetotransport measurements, we performed a comprehensive investigation on $MoAs_2$, which is isostructural to the $TmPn_2$ series of compounds and also exhibits near-quadratic XMR. We reveal a relatively simple bulk band structure agreeing with the predictions and the existence of a trivial massless surface state along $\bar{\Gamma}$-$\bar{X}$. Intriguingly, the observed Fermi surfaces (FSs) in $MoAs_2$ are dominated by an open-orbit topology, rather than closed pockets. We then scrutinize the angular-dependent magnetoresistance together with three-dimensional electronic structure of $MoAs_2$. Based on these results, the origin of the near-quadratic XMR in $MoAs_2$ is possibly ascribed to the carriers motion on the FSs with dominant open-orbit topology by examining the proposed mechanisms in other XMR semimetals.

PACS numbers: 73.20.At, 71.18.+y, 79.60.-i

The emergence of novel states in condensed matter is not only classified by the typical spontaneous symmetry breaking, but also by their topology, i.e., the topologically protected quantum states [1–3]. The discovery of such symmetry protected states of matter in two-dimensional (2D) [4–6] and three-dimensional (3D) topological insulators (TIs) [7], node-line semimetals [8, 9], topological crystalline insulators [10, 11], and Dirac and Weyl semimetals [12–17], has attracted tremendous interests in condensed matter physics and material science. The magnetotransport behavior of these topological quantum states is often unusual, such as linear transverse magnetoresistance (MR) and negative longitudinal MR in Dirac and Weyl semimetals [18–24], and more generally, extremely large transverse MR (XMR) in nonmagnetic semimetals [25–30]. On the fundamental research side, MR can give information about the characteristics of electronic structures and spin structures. It also provides promising potential and candidates for magnetic memory, magnetic field sensors, and other spintronics devices.

Recently, the discovery of XMR in a class of transition metal dipnictides $TmPn_2$ (Tm = Ta, Nb; Pn = P, As, Sb) [31–36] has sparked immense interests for understanding the underlying mechanism of quadratic XMR and exploring novel quantum states arising from nontrivial topology. Two most remarkable characteristics of magnetotransport behavior in the $TmPn_2$ series are the near-quadratic field dependence of MR and a field-induced up-turn in resistivity followed by a plateau at low temperatures, similar to the Dirac and Weyl semimetals, which, nevertheless, display a linear MR distinct from the near-quadratic behavior [18–21]. Additionally, the appearance of negative longitudinal MR, which serves as a common signature in Weyl semimetals [20, 23], is seemingly materials dependent in the $TmPn_2$ series [32, 37, 38]. All these features indicate a distinct and rich electronic and topological property beyond the known TIs and topological semimetals. Another two series of semimetals possessing quadratic XMR behavior and rich topological characteristics are the ZrSiS family [39–41] and LnX (Ln = La, Y, Nd, or Ce; X = Sb/Bi) series [42–48], whose electronic structures have been considerably studied both in theory and experiment [49–55]. While the band structures of the $TmPn_2$ series have been theoretically characterized in several work [32–34, 56], experimental observations have not yet been reported. It is widely believed that the large positive MR in semimetals is intimately related to their underlying electronic structures. Therefore, a systematic and unambiguous experimental study on the electronic structure of the $TmPn_2$ series of compounds is urgently demanded for understanding the origin of quadratic XMR and exploring novel topological phases. Eventually, we suggest the open-orbit FS topology as another candidate mechanism to explain the XMR behavior, in addition to the earlier proposed origins like electron-hole resonance compensation [57], nontrivial band topology [42], and forbidden backscattering at zero field [58].

In this Letter, we employ systematic angle-resolved photoemission spectroscopy (ARPES) and magnetotransport mea-

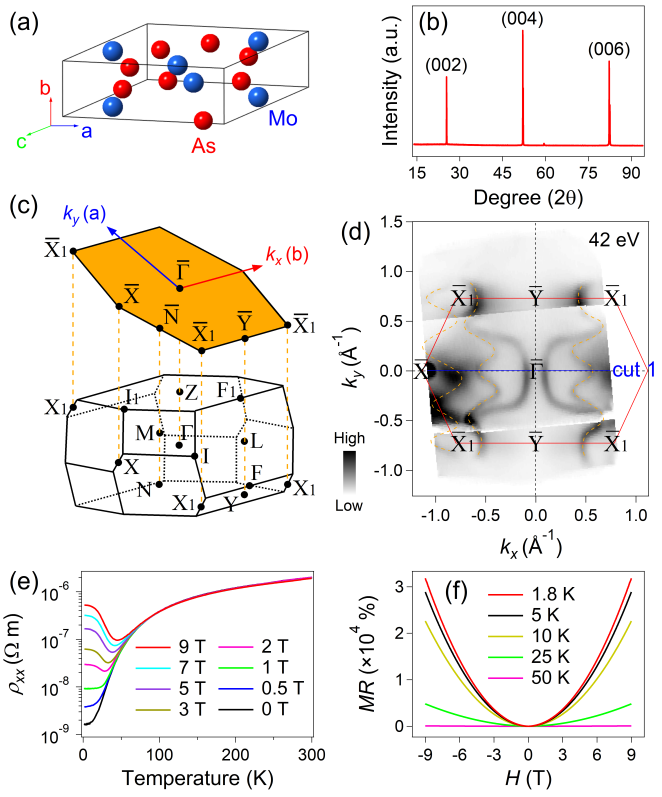

FIG. 1: Crystal structure, FS topology, and magnetotransport of $MoAs_2$. (a) Schematic crystal structure of $MoAs_2$. (b) XRD pattern on the (001) surface. (c) Schematic primitive BZ and corresponding 2D projected BZ of the (001) surface. The reciprocal lattice vectors (k_x, k_y) of (001)-projected BZ and crystal axes (a, b) are indicated. (d) Constant energy ARPES image of $MoAs_2$ obtained by $h\nu = 42$ eV at E_F. Cut 1 indicates the momentum location of the measured bands in Figs. 2(a) and 2(b). Red lines represent the (001) surface BZ. Orange dashed curves are guides to the eye for the "double ripple"-shaped FSs. (e) Temperature dependence of the resistivity in magnetic fields (H = 0, 0.5, 1, 2, 3, 5, 7, and 9 T). The magnetic field is parallel to the [001] direction and the electric current is parallel to the [010] direction. (f) $MR\,(\%) = [R(H) - R(0)]/R(0) \times 100\,\%$ plotted as a function of magnetic field at temperatures from 1.8 K to 50 K.

surements on single crystals of $MoAs_2$, which is isostructural to the $TmPn_2$ series of compounds and exhibits quadratic MR exceeding 3.2×10^4% at 1.8 K under 9-T magnetic field. We reveal a rather simple band structure around E_F on the (001) surface of $MoAs_2$. The Fermi surface (FS) topology is clearly resolved to display two "double ripple"-shaped hole-like FSs extending along the [100] direction, which do not close along the [001] direction either, and one electron FS pocket at $\bar{X}$. Besides, we identify two "handle"-like FSs around $\bar{\Gamma}$, which arise from a trivial massless surface state (SS) along $\bar{\Gamma}$-$\bar{X}$ by comparing with first-principles calculations. The dominant open-orbit FS topology and electron pocket at $\bar{X}$ are responsible for the anisotropy of MR. As compared to other compounds of the $TmPn_2$ family, $MoAs_2$ has a much simpler electronic structure, which facilitates the investigation on the underlying mechanism of quadratic XMR.

High-quality single crystals of $MoAs_2$ with large residual resistance ratio [RRR = R(300 K)/R(1.8 K) = 1238] were grown via the chemical vapor transport method. The Vienna *ab initio* Simulation Package with the generalized gradient approximation of Perdew-Burke-Ernzerhof type exchange correlation potential is employed in our first-principles calculations. The Mo atoms are located at Wyckoff positions 4*i* (0.154, 0, 0.2) and the As atoms are located at Wyckoff positions 4*i* (0.143, 0, 0.531) and 4*i* (0.399, 0, 0.112), respectively. The plane-wave cutoff energy is 375 eV and the k-point sampling grids in the self-consistent process is 11×11×11. Spin-orbit coupling is taken into account in all the above calculations. ARPES measurements were performed at the Dreamline beamline of the Shanghai Synchrotron Radiation Facility (SSRF) with a Scienta D80 analyzer. The energy and angular resolutions were set to 15 meV and 0.2°, respectively. All samples were cleaved *in situ* along the (001) plane and measured at T = 20 K in a working vacuum better than 5×10^{-11} Torr.

$MoAs_2$ crystallizes in a monoclinic structure with space group $C2/m$ (No. 12), as illustrated in Fig. 1(a) [59]. It is isostructural to the well known $TmPn_2$ family. Figure 1(b) shows the x-ray diffraction (XRD) patterns recorded on single crystals measured by ARPES, indicating our measurements were performed on the (001) plane. The schematic 3D Brillouin zone (BZ) of the primitive cell and the corresponding 2D projected BZ of the (001) surface are presented in Fig. 1(c). In Fig. 1(d), one can see the FSs measured with photon energy $h\nu = 42$ eV exhibiting obvious modulations along k_y. We observe two "double ripple"-shaped hole-like FSs elongated along the [100] direction near the BZ boundary $\bar{X}$ and $\bar{X}_1$, one electron pocket at $\bar{X}$, as well as two "handle"-like FSs around $\bar{\Gamma}$. By further comparing with the calculated bulk band dispersions illustrated in Fig. 2, one can identify that the "handle"-like FSs are not of bulk origin, but rather derive from SSs as discussed in the following.

Figure 1(e) is the temperature evolution of the resistivity taken with different magnetic fields that are aligned along the [001] direction, perpendicular to the [010] direction of electric currents. $MoAs_2$ shows the metallic behavior from 1.8 K to 300 K without magnetic field. When the 9-T magnetic field is applied, one can see a prominent up-turn and a saturation at low temperatures. As depicted in Fig. 1(f), $MoAs_2$ exhibits rather large MR exceeding 3.2×10^4% at 1.8 K under 9-T magnetic field, and there is a drastic suppression of MR with increasing temperature. One can obtain a nearly-quadratic exponent m = 1.97 by fitting the MR-H profile at 1.8 K with a power-law function. These fingerprints are consistent with the common features of XMR semimetals [57].

In order to uncover the underlying nature of quadratic XMR and topological characteristics in $MoAs_2$, we investigate the near-E_F band dispersions along the high-symmetry lines $\bar{\Gamma}$-$\bar{X}$ and $\bar{Y}$-$\bar{X}_1$. The band structure along $\bar{\Gamma}$-$\bar{X}$ is presented in Figs.

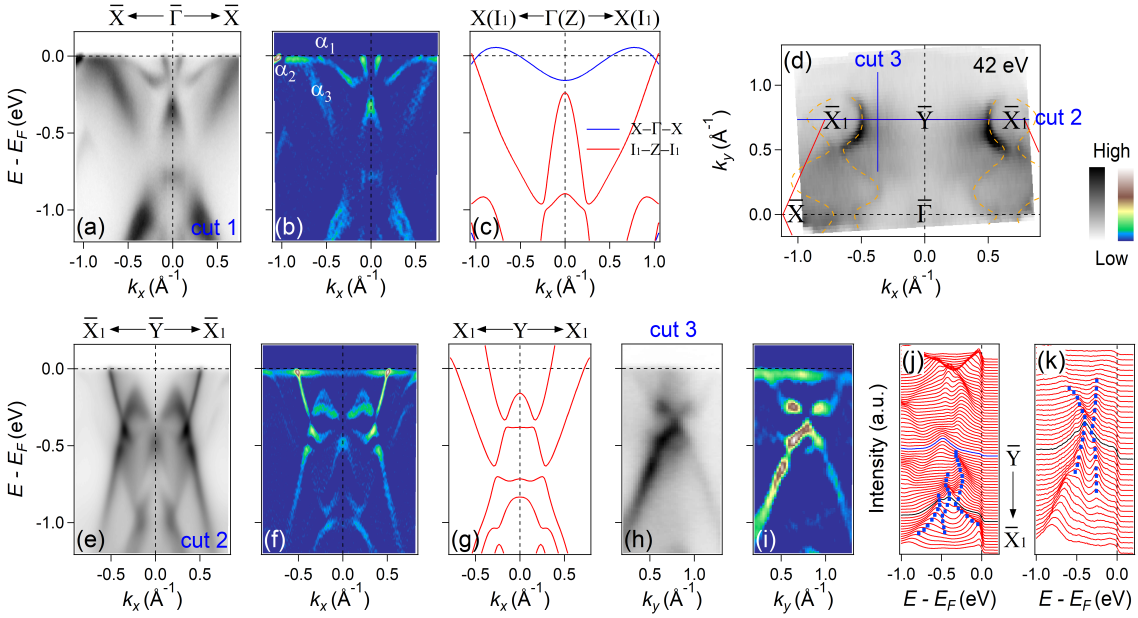

FIG. 2: Near-E_F band dispersions along high-symmetry lines of $MoAs_2$. (a),(b) Photoemission intensity plot and corresponding second derivative plot along $\bar{\Gamma}$-$\bar{X}$ [cut 1 in Fig. 1(d)], respectively. (c) Calculated band structures along Γ-X and Z-I_1, as illustrated by blue and red curves, respectively, considering that the X and I_1 points are approximately projected to one point on the (001) surface. (d) FS intensity plot obtained by integrating the spectral weight within E_F±10 meV recorded with $h\nu$ = 42 eV, focusing around $\bar{Y}$ point. Cuts 2 and 3 indicate the momentum locations of the experimental band structures in (e)-(k). Red lines represent the (001) surface BZ. Orange dashed curves are guides to the eye for the "double ripple"-shaped FSs. (e),(f) Same as (a),(b) but along $\bar{Y}$-$\bar{X}_1$ [cut 2 in (d)]. (g) Calculated band structure along Y-X_1. (h),(i) Same as (a),(b) but along cut 3 in (d). (j),(k) EDC plots of (e),(h), respectively. The band gap is highlighted by black curves. Blue dots are extracted peak positions, serving as guides to the eye.

2(a)-2(c). As shown in Figs. 2(a) and 2(b), we identify one Dirac conelike band centered at $\bar{\Gamma}$ that will be discussed below. Three additional bands crossing E_F are clearly distinguished. The innermost electron band (α_1) disperses slowly and crosses E_F at $k_x \sim$ -0.58 Å^{-1}, forming the inner "ripple"-shaped FS, then it turns back as the outmost electron band (α_2), which is in agreement with the bulk band calculations along Γ-X depicted in Fig. 2(c). As the absence of the middle one (α_3), which forms the outer "ripple"-shaped FS, in the calculations along Γ-X, we suggest that α_3 may not come from the $k_z \sim 0$ plane. We further perform bulk band calculations along Z-I_1 as shown in Fig. 2(c). The consistency between α_3 and the calculations helps finding out the origin of this band.

We investigate the electronic structure along $\bar{Y}$-$\bar{X}_1$ in Figs. 2(e)-2(k) to examine the origin of the "double ripple"-shaped FSs elongated along the [100] direction. As indicated in Fig. 2(d), the "double ripple"-shaped feature can be resolved more clearly from the FS mapping focusing around the $\bar{Y}$ point, while the "handle"-like FSs are relatively weak in this geometry due to the matrix element effect. From the measured band dispersions along $\bar{Y}$-$\bar{X}_1$ illustrated in Figs. 2(e) and 2(f), one can observe two almost linearly dispersive bands crossing E_F, which correspond to the inner and outer part of the "double ripple"-shaped FSs, respectively. The experimental band structures agree well with the bulk band calculations along Y-X_1 shown in Fig. 2(g). As the k_z momentum of the bulk Y-X_1 direction is near the $k_z \sim \pi$ plane, the electron band corresponding to the outer "ripple"-shaped FS can be identified from the bulk calculations in Fig. 2(g), just like the situation for α_3 captured by the calculations along Z-I_1 [53, 54]. The theoretical calculations in Fig. 2(g) clearly indicate the existence of a band gap between the above two linearly dispersing bands. To further capture this gap, we plot the band dispersions perpendicular to $\bar{Y}$-$\bar{X}_1$ at the momentum of the band gap, i.e., $k_x \sim$ -0.37 Å^{-1}, in Figs. 2(h) and 2(i). It is clear that the gap is more prominent from this view. We then systematically investigate the energy distribution curves (EDCs) of Figs. 2(e) and 2(h), as displayed in Figs. 2(j) and 2(k), respectively, the fine details of the gap (~80 meV) can be unambiguously identified.

To illuminate the origin of the "handle"-like FSs around $\bar{\Gamma}$, we investigate the band dispersions recorded with different photon energies. As discussed in the above, while most experimental band structures along $\bar{\Gamma}$-$\bar{X}$ are in agreement with the bulk band calculations [Fig. 2(c)], we observe an extra Dirac conelike band centered at $\bar{\Gamma}$, corresponding to the two "handle"-like curves in the FS intensity map. We show the constant energy plot in the k_x-k_z plane at k_y = 0 at E_F

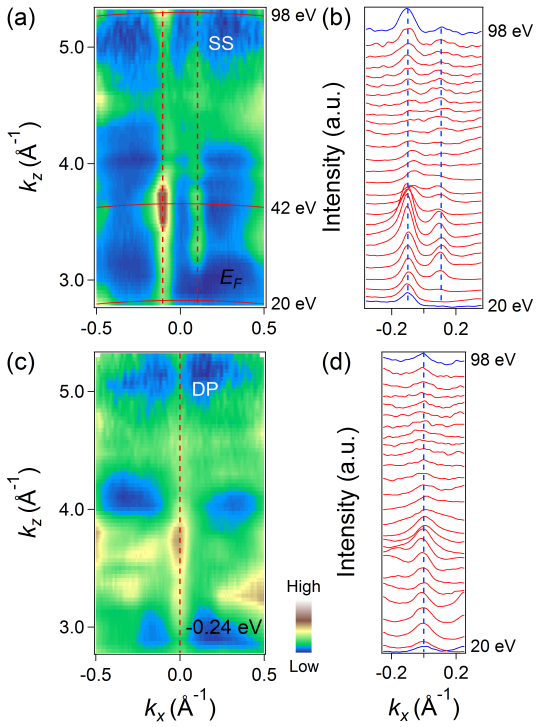

FIG. 3: Photon-energy-dependent spectra along $\bar{\Gamma}$-$\bar{X}$ of $MoAs_2$. (a) ARPES intensity map at E_F in the k_x-k_z plane at k_y = 0 recorded with photon energies from 20 to 98 eV. Red curves from bottom to top indicate the momentum locations taken at $h\nu$ = 20, 42, and 98 eV, respectively. (b) MDC plot of (a) around the BZ center. (c) Same as (a) but at E = -0.24 eV. (d) MDC plot of (c) around the BZ center. Red and blue dashed lines in (a),(b) and (c),(d) show the Fermi crossings and the DP of the SS around $\bar{\Gamma}$, where identifiable, respectively.

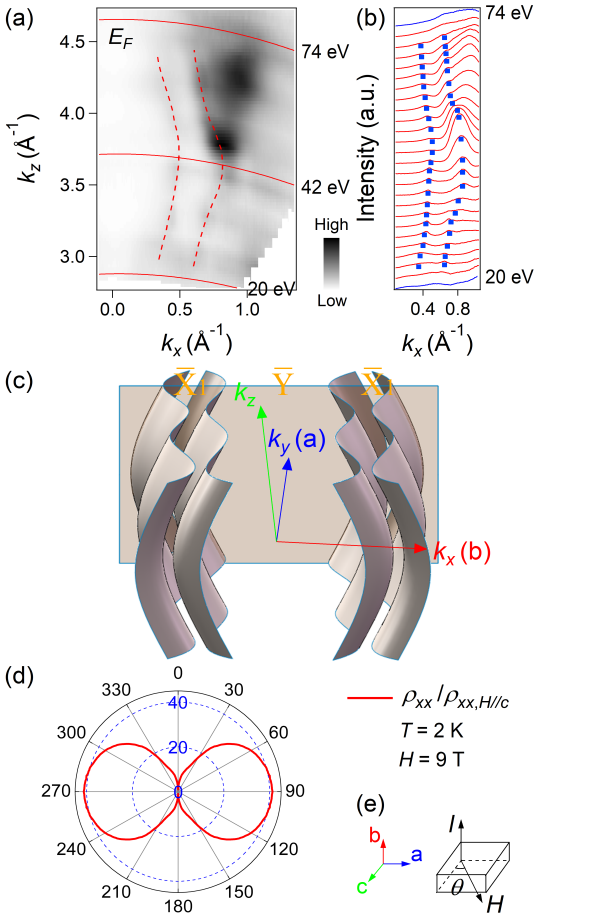

FIG. 4: Photon-energy-dependent spectra along $\bar{Y}$-$\bar{X}_1$ and angular-dependent MR of $MoAs_2$. (a) ARPES intensity map at E_F in the k_x-k_z plane at $k_y = \pi$ recorded with various photon energies. Red curves from bottom to top indicate the momentum locations taken at $h\nu$ = 20, 42, and 74 eV, respectively. (b) MDC plot of (a). Red dashed curves in (a) and blue dots in (b), which are extracted peak positions, indicate the Fermi crossings of k_z bandmap. (c) Schematic diagram of the open-orbit FS topology extending in the 3D BZ. The translucent plane indicates the momentum location of the k_x-k_z mapping in (a). (d) Polar plot of ρ_{xx} at T = 2 K and H = 9 T, normalized by ρ_{xx} for $H \parallel c$, as a function of the magnetic field angle θ defined in (e). (e) Schematic illustration for the direction of H and I in the angular-dependent MR measurements, where $\theta = 0^\circ$ corresponds to $H \parallel c$.

and E = -0.24 eV, which is the binding energy of the Dirac point (DP) at $\bar{\Gamma}$, in Figs. 3(a) and 3(c), respectively. The momentum distribution curve (MDC) plots of the photon-energy-dependence ARPES bandmap [Figs. 3(a) and 3(c)] focusing around the massless Dirac-like band are presented in Figs. 3(b) and 3(d), respectively. The Dirac-like band features, including the Fermi crossings and the DP, do not show noticeable change with a varying photon energy over a wide range, confirming that it is a SS.

In order to resolve the relevance between quadratic XMR and underlying electronic structure in $MoAs_2$, we further perform k_z-dependent measurements along $\bar{Y}$-$\bar{X}_1$ focusing on the "double ripple"-shaped FSs. The photon energy variation covers more than one BZ along the k_z direction ($\sim$ 0.88 Å^{-1}), which is sufficient to illustrate the periodicity along k_z. As shown in Figs. 4(a) and 4(b), the "double ripple"-shaped open FSs do not close along the k_z direction either. When the FS topology contains open orbits along certain directions, MR in materials is not saturated and parabolically dependent on the magnetic field [60, 61]. To elucidate the possible electronic origin of the quadratic XMR in $MoAs_2$, i.e., the carriers motion on the FSs with dominant open-orbit topology, angular-dependent MR measurements were carried out. As depicted in Fig. 4(e), the magnetic field is tilted within the ac-plane from $H \parallel c$ ($\theta = 0^\circ$) to $H \perp c$ ($\theta = 90^\circ$), the electric current is applied along the b-axis. Figure 4(d) illustrates the polar plot of $\rho_{xx}/\rho_{xx}(H \parallel c)$ under H = 9 T and T = 2 K, where a dumbbell-like pattern with two-fold symmetry can be clearly seen.

So far, immense work has been generated on the origin of

quadratic XMR behavior, and several mechanisms have been proposed, including electron-hole resonance compensation [57], nontrivial band topology [42], and forbidden backscattering at zero field [58]. The Z_2 classification is (0; 000) based on our first-principles calculations, demonstrating that $MoAs_2$ is a topologically trivial material. The inversion symmetry in $MoAs_2$ is preserved and its spins are doubly degenerate at zero field. Therefore, the latter two explanations are not applicable to $MoAs_2$. While electron-hole resonance compensation can be broadly applied in many XMR semimetals with closed FS trajectories based on the two-band model [43, 53, 57, 62], its availability in XMR materials with open-orbit FS topology is still unclear and further work is required [63]. Under the influence of a magnetic field, carriers in clean materials with closed FSs will travel several orbits before getting scattered, resulting in velocity average to zero in the plane perpendicular to the magnetic field. This contrasts with carriers on open FSs, for which the product of the cyclotron frequency and the relaxation time is no longer much larger than 1, thus leading to a finite in-plane velocity. This would significantly enhance the MR and lead to a quadratic-like dependence on the magnetic field [60, 61]. Hence, we conjecture that the quadratic XMR in $MoAs_2$ is attributed to the carriers motion on the FSs with dominant open-orbit topology. Similar XMR behavior related to the open-orbit topology at FSs along certain directions has also been reported in $PdCoO_2$ and ZrSiS [64, 65].

According to our measured band structure of $MoAs_2$, when turning the direction of the magnetic field within the *ac*-plane, the perpendicular cross-section of the FSs remains open throughout the full range, whereas the resistivity still displays prominent anisotropy in Fig. 4(d). Considering the SS origin of the "handle"-like FSs around $\bar{\Gamma}$, the suppression of MR when the field is rotated towards *c*-axis might result from the carriers with remarkably heavy effective masses performing cyclotronic motion on the electron pocket at $\bar{X}$.

In conclusion, our systematic ARPES and magnetotransport measurements on XMR semimetal $MoAs_2$ reveal a relatively simple electronic structure contrasting to those typically expected for other compounds of the $TmPn_2$ series. Intriguingly, the observed FSs are dominated by two "double ripple"-shaped FSs around the BZ boundary, showing open-orbit topology along both the [100] and [001] directions. We identify two "handle"-like FSs around $\bar{\Gamma}$ and demonstrate their SS origin. Based on detailed electronic structure analysis, we attribute the possible origin of quadratic XMR in $MoAs_2$ to the carriers motion on the FSs with dominant open-orbit topology, serving as another candidate mechanism for XMR in semimetals.

We would like to thank H. C. Lei, T.-L. Xia for fruitful discussions, and Y.-Y. Wang, S.-S. Sun for the help in transport measurements. This work was supported by the Ministry of Science and Technology of China (Programs No. 2013CB921700, No. 2015CB921000, No. 2016YFA0300300, No. 2016YFA0300600, No. 2016YFA0302400, and No. 2016YFA0401000), the National Natural Science Foundation of China (Grants No. 11274381, No. 11274362, No. 11474340, No. 11234014, No. 11274367, No. 11474330, and No. 11674371), and the Chinese Academy of Sciences (CAS) (Project No. XDB07000000). R.L. and K.L. were supported by the Fundamental Research Funds for the Central Universities, and the Research Funds of Renmin University of China (RUC) (Grants No. 17XNH055 and No. 14XNLQ03). Y.H. was supported by the CAS Pioneer Hundred Talents Program.

R. L., Y. F. X., L.-X. Z., and Z.-Q. H. contributed equally to this work.

* Electronic address: scw@ruc.edu.cn

[1] M. Z. Hasan and C. L. Kane, Rev. Mod. Phys. **82**, 3045 (2010).
[2] X. L. Qi and S. C. Zhang, Rev. Mod. Phys. **83**, 1057 (2011).
[3] H. Weng, X. Dai, and Z. Fang, MRS Bulletin **39**, 849 (2014).
[4] B. A. Bernevig, T. L. Hughes, and S. C. Zhang, Science **314**, 1757 (2006).
[5] M. König, S. Wiedmann, C. Brüne, A. Roth, H. Buhmann, L. W. Molenkamp, X.-L. Qi, and S.-C. Zhang, Science **318**, 766 (2007).
[6] I. Knez, R.-R. Du, and G. Sullivan, Phys. Rev. Lett. **107**, 136603 (2011).
[7] Y. L. Chen, J. G. Analytis, J.-H. Chu, Z. K. Liu, S.-K. Mo, X. L. Qi, H. J. Zhang, D. H. Lu, X. Dai, Z. Fang, S. C. Zhang, I. R. Fisher, Z. Hussain, and Z.-X. Shen, Science **325**, 178 (2009).
[8] A. A. Burkov, M. D. Hook, and L. Balents, Phys. Rev. B **84**, 235126 (2011).
[9] R. Yu, H. M. Weng, Z. Fang, X. Dai, and X. Hu, Phys. Rev. Lett. **115**, 036807 (2015).
[10] L. Fu, Phys. Rev. Lett. **106**, 106802 (2011).
[11] T. H. Hsieh, H. Lin, J. Liu, W. Duan, A. Bansil, and L. Fu, Nat. Commun. **3**, 982 (2012).
[12] Z. Wang, Y. Sun, X.-Q. Chen, C. Franchini, G. Xu, H. Weng, X. Dai, and Z. Fang, Phys. Rev. B **85**, 195320 (2012).
[13] Z. K. Liu, B. Zhou, Y. Zhang, Z. J. Wang, H. Weng, D. Prabhakaran, S.-K.Mo, Z. X. Shen, Z. Fang, X. Dai, Z. Hussain, and Y. L. Chen, Science **343**, 864 (2014).
[14] H. Weng, C. Fang, Z. Fang, B. A. Bernevig, and X. Dai, Phys. Rev. X **5**, 011029 (2015).
[15] B. Q. Lv, H. M. Weng, B. B. Fu, X. P. Wang, H. Miao, J. Ma, P. Richard, X. C. Huang, L. X. Zhao, G. F. Chen, Z. Fang, X. Dai, T. Qian, and H. Ding, Phys. Rev. X **5**, 031013 (2015).
[16] S. Huang, S. Xu, I. Belopolski, C. Lee, G. Chang, B. Wang, N. Alidoust, G. Bian, M. Neupane, C. Zhang, S. Jia, A. Bansil, H. Lin, and M. Z. Hasan, Nat. Commun. **6**, 7373 (2015).
[17] S. Xu, I. Belopolski, N. Alidoust, Madhab Neupane, G. Bian, C. Zhang, R. Sankar, G. Chang, Z. Yuan, C. Lee, S. Huang, H. Zheng, J. Ma, D. S. Sanchez, B. Wang, A. Bansil, F. Chou, P. P. Shibayev, H. Lin, S. Jia, and M. Z. Hasan, Science **349**, 613 (2015).
[18] J. Feng, Y. Pang, D. Wu, Z. Wang, H. Weng, J. Li, X. Dai, Z. Fang, Y. Shi, and L. Lu, Phys. Rev. B **92**, 081306 (2015).
[19] T. Liang, Q. Gibson, M. N. Ali, M. Liu, R. J. Cava, and N. P. Ong, Nat. Mater. **14**, 280 (2015).
[20] X. C. Huang, L. X. Zhao, Y. J. Long, P. P. Wang, D.Chen, Z. H. Yang, H. Liang, M. Q. Xue, H. M. Weng, Z. Fang, X. Dai, and G. F. Chen, Phys. Rev. X. **5**, 031023 (2015).
[21] C. Shekhar, A. K. Nayak, Y. Sun, M. Schmidt, M. Nicklas, I. Leermakers, U. Zeitler, Z. K. Liu, Y. L. Chen, W. Schnelle, J.

Grin, C. Felser, and B. H. Yan, Nat. Phys. **11**, 645 (2015).
[22] J. Xiong, S. K. Kushwaha, T. Liang, J. W. Krizan, M. Hirschberger, W. Wang, R. J. Cava, and N. P. Ong, Science **350**, 413 (2015).
[23] C. Zhang, S.-Y. Xu, I. Belopolski, Z. Yuan, Z. Lin, B. Tong, N. Alidoust, C.-C. Lee, S.-M. Huang, H. Lin, M. Neupane, D. S. Sanchez, H. Zheng, G. Bian, J. Wang, C. Zhang, T. Neupert, M. Z. Hasan, and S. Jia, Nat. Commun. **7**, 10735 (2016).
[24] C-Z. Li, L. Wang, H. W. Liu, J. Wang, Z.-M. Liao, and D.-P. Yu, Nat. Commun. **6**, 10137 (2015).
[25] L. Schubnikow, and W. J. De Haas, Nature (London) **126**, 500 (1930).
[26] P. B. Alers, and R. T. Webber, Phys. Rev. **84**, 863 (1951).
[27] T. Kasuya, M. Sera, and T. Suzuki, J. Phys. Soc. Jpn. **62**, 2561 (1993).
[28] F. Y. Yang, K. Liu, K. Hong, D. H. Reich, P. C. Searson, and C. L. Chein, Science **284**, 1335 (1999).
[29] R. Xu, A. Husmann, T.F. Rosenbaum, M.-L. Saboungi, J. E. Enderby, and P. B. Littlewood, Nature (London) **390**, 57 (1997).
[30] E. Mun, H. Ko, G. J. Miller, G. D. Samolyuk, S. L. Budko, and P. C. Canfield, Phys. Rev. B **85**, 035135 (2012).
[31] K. Wang, D. Graf, L. Li, L. Wang, and C. Petrovic, Sci. Rep. **4**, 7328 (2014).
[32] B. Shen, X. Y. Deng, G. Kotliar, and N. Ni, Phys. Rev. B **93**, 195119 (2016).
[33] D. S. Wu, J. Liao, W. Yi, X. Wang, P. G. Li, H. M. Weng, Y. G. Shi, Y. Q. Li, J. L. Luo, X. Dai, and Z. Fang, Appl. Phys. Lett. **108**, 042105 (2016).
[34] C. C. Xu, J. Chen, G. X. Zhi, Y. K. Li, J. H. Dai, and C. Cao, Phys. Rev. B **93**, 195106 (2016).
[35] Y.-Y. Wang, Q.-H. Yu, P.-J. Guo, K. Liu, and T.-L. Xia, Phys. Rev. B **94**, 041103 (2016).
[36] Z. Wang, Y. Li, Y. Lu, Z. Shen, F. Sheng, C. Feng, Y. Zheng, and Z. A. Xu, arXiv:1603.01717.
[37] Y. Li, L. Li, J. Wang, T. Wang, X. Xu, C. Xi, C. Cao, and J. Dai, Phys. Rev. B **94**, 121115(R) (2016).
[38] Y. P. Li, Z. Wang, Y. Lu, X. Yang, Z. Shen, F. Sheng, C. Feng, Y. Zheng, Z. A. Xu, arXiv:1603.04056.
[39] R. Singha, A. Pariari, B. Satpati, and P. Mandal, Proc. Natl. Acad. Sci. **114**, 2468 (2017).
[40] M. N. Ali, L. M. Schoop, C. Garg, J. M. Lippmann, E. Lara, B. Lotsch, and S. Parkin, arXiv:1603.09318.
[41] X. F. Wang, X. C. Pan, M. Gao, J. H. Yu, J. Jiang, J. R. Zhang, H. K. Zuo, M. H. Zhang, Z. X. Wei, W. Niu, Z. C. Xia, X. G. Wan, Y. L. Chen, F. Q. Song, Y. B. Xu, B. G. Wang, G. H. Wang, and R. Zhang, Adv. Electron. Mater. **2**, 1600228 (2016).
[42] F. F. Tafti, Q. D. Gibson, S. K. Kushwaha, N. Haldolaarachchige, and R. J. Cava, Nat. Phys. **12**, 272 (2015).
[43] S. S. Sun, Q. Wang, P. J. Guo, K. Liu, and H. C. Lei, New J. Phys. **18**, 082002 (2016).
[44] N. Kumar, C. Shekhar, S.-C. Wu, I. Leermakers, O. Young, U. Zeitler, B. H. Yan, and C. Felser, Phys. Rev. B **93**, 241106(R) (2016).
[45] Q. Yu, Y. Wang, R. Lou, P. Guo, S. Xu, K. Liu, S.-C. Wang, and T.-L. Xia, arXiv:1604.05912.
[46] O. Pavlosiuk, P. Swatek, and P. Wiśniewski, Sci. Rep. **6**, 38691 (2016).
[47] N. Wakeham, E. D. Bauer, M. Neupane, and F. Ronning, Phys. Rev. B **93**, 205152 (2016).
[48] N. Alidoust, A. Alexandradinata, S.-Y. Xu, I. Belopolski, S. K. Kushwaha, M. Zeng, M. Neupane, G. Bian, C. Liu, D. S. Sanchez, P. P. Shibayev, H. Zheng, L. Fu, A. Bansil, H. Lin, R. J. Cava, and M. Z. Hasan, arXiv:1604.08571.
[49] Q. N. Xu, Z. Song, S. Nie, H. M. Weng, Z. Fang, and X. Dai, Phys. Rev. B **92**, 205310 (2015).
[50] R. Lou, J.-Z. Ma, Q.-N. Xu, B.-B. Fu, L.-Y. Kong, Y.-G. Shi, P. Richard, H.-M. Weng, Z. Fang, S.-S. Sun, Q. Wang, H.-C. Lei, T. Qian, H. Ding, and S.-C. Wang, Phys. Rev. B **93**, 241104(R) (2016).
[51] L. M. Schoop, M. N. Ali, C. Straβer, A. Topp, A. Varykhalov, D. Marchenko, V. Duppel, S. S. P. Parkin, B. V. Lotsch, and C. R. Ast, Nat. Commun. **7**, 11696 (2016).
[52] M. Zeng, C. Fang, G. Chang, Y.-A. Chen, T. Hsieh, A. Bansil, H. Lin, and L. Fu, arXiv:1504.03492.
[53] L.-K. Zeng, R. Lou, D.-S. Wu, Q. N. Xu, P.-J. Guo, L.-Y. Kong, Y.-G. Zhong, J.-Z. Ma, B.-B. Fu, P. Richard, P. Wang, G. T. Liu, L. Lu, Y.-B. Huang, C. Fang, S.-S. Sun, Q. Wang, L. Wang, Y.-G. Shi, H. M. Weng, H.-C. Lei, K. Liu, S.-C. Wang, T. Qian, J.-L. Luo, and H. Ding, Phys. Rev. Lett. **117**, 127204 (2016).
[54] R. Lou, B.-B. Fu, Q. N. Xu, P.-J. Guo, L.-Y. Kong, L.-K. Zeng, J.-Z. Ma, P. Richard, C. Fang, Y.-B. Huang, S.-S. Sun, Q. Wang, L. Wang, Y.-G. Shi, H. C. Lei, K. Liu, H. M. Weng, T. Qian, H. Ding, and S.-C. Wang, Phys. Rev. B **95**, 115140 (2017).
[55] P.-J. Guo, H.-C. Yang, B.-J. Zhang, K. Liu, and Z.-Y. Lu, Phys. Rev. B **93**, 235142 (2016).
[56] Y. K. Luo, R. D. McDonald, P. F. S. Rosa, B. Scott, N. Wakeham, N. J. Ghimire, E. D. Bauer, J. D. Thompson, and F. Ronning, Sci. Rep. **6**, 27294 (2016).
[57] M. N. Ali, J. Xiong, S. Flynn, J. Tao, Q. D. Gibson, L. M. Schoop, T. Liang, N. Haldolaarachchige, M. Hirschberger, N. P. Ong, and R. J. Cava, Nature (London) **514**, 205 (2014).
[58] J. Jiang, F. Tang, X. C. Pan, H. M. Liu, X. H. Niu, Y. X. Wang, D. F. Xu, H. F. Yang, B. P. Xie, F. Q. Song, P. Dudin, T. K. Kim, M. Hoesch, P. K. Das, I. Vobornik, X. G. Wan, and D. L. Feng, Phys. Rev. Lett. **115**, 166601 (2015).
[59] J. Wang, L. Li, W. You, T. Wang, C. Cao, J. Dai, and Y. Li, arXiv:1610.08594.
[60] A. A. Abrikosov, *Fundamentals of the Theory of Metals* (North-Holland, 1988).
[61] J. Singleton, *Band Theory and Electronic Properties of Solids* (Oxford University Press, 2001).
[62] A. B. Pippard, *Magnetoresistance in Metals* (Cambridge University Press, Cambridge, 1989).
[63] N. W. Ashcroft and N. D. Mermin, *Solid Sate Physics* (Holt, Rinehart and Winston, New York, 1976).
[64] H. Takatsu, J. J. Ishikawa, S. Yonezawa, H. Yoshino, T. Shishidou, T. Oguchi, K. Murata, and Y. Maeno, Phys. Rev. Lett. **111**, 056601 (2013).
[65] Y.-Y. Lv, B.-B. Zhang, X. Li, S.-H. Yao, Y. B. Chen, J. Zhou, S.-T. Zhang, M.-H. Lu, and Y.-F. Chen, Appl. Phys. Lett. **108**, 244101 (2016).